Bioorganic Chemistry 163 (2025) 108715

Contents lists available at ScienceDirect

Bioorganic Chemistry

journal homepage: www.elsevier.com/locate/bioorg

Fragments of cathelicidins PMAP-36 and BMAP-27 and their *D*-enantiomers: Effects of all *D* substitutions on structure, protease resistance and antimicrobial properties

Francesca Albini [a], Barbara Biondi [b], Adriana Di Stasi [a,c], Andrea Schivo [a], Mario Mardirossian [c], Marco Scocchi [c], Cristina Peggion [a,b,*]

[a] *Department of Chemical Sciences, University of Padova, Padova, Italy*
[b] *Institute of Biomolecular Chemistry, Padova Unit, CNR, Padova, Italy*
[c] *Department of Life Sciences, University of Trieste, Trieste, Italy*

ARTICLE INFO

Keywords:
PMAP-36
BMAP-27
BMAP(1–18)
D-enantiomer
Antimicrobial peptide
Cathelicidin

ABSTRACT

Antimicrobial peptides (AMPs) are natural molecules of great interest in the fight against bacteria and in addressing antibiotic resistance. Their use as antimicrobial drugs is still limited due to their cytotoxicity and poor resistance to proteolysis. PMAP-36 and BMAP-27 are cathelicidins that contribute to innate immunity.

Two short sequences, PMAP(12–24) and BMAP(1–18), are the most promising analogues identified but despite their broad antibacterial activity, they undergo rapid proteolytic degradation.

In this study, the *D* and *L* enantiomers of the two peptides were synthesised, and their structures were elucidated and compared by circular dichroism (CD) spectroscopy and 2D-NMR analysis. Conformational studies revealed that, despite their short sequence, all peptides adopted helical structures in membrane-mimetic environments, with subtle differences between the two AMP groups, PMAP(12–24) being more prone to adopt a mixed $\alpha/3_{10}$-helical conformation ($R([\Theta]_{222}/[\Theta]_{206} = 0.4–0.5$) and BMAP(1–18) being closer to a pure α-helix ($R([\Theta]_{222}/[\Theta]_{208} = 0.7–0.8$). These structural differences between the two peptides were found to influence their antimicrobial activity and mode of membrane permeabilization. Moreover, the *D* enantiomers of both analogues were resistant to proteolysis. All peptides showed a broad spectrum of antibacterial activity (main MIC range: 1–16 μM). Cytotoxicity studies in fibroblast showed that the peptides were non-cytotoxic at concentrations corresponding to their antibacterial activity. Overall, this study led to the identification of structurally interesting short peptides that could serve as prototypes for the development of effective and practical antibacterial drugs.

1. Introduction

The rapid rise of antibiotic-resistant bacteria is a global crisis, threatening the effectiveness of antibiotic therapy, that revolutionised medicine and saved countless lives. Decades after antibiotics were first used to treat patients, bacterial infections are again becoming a major risk [1,2]. Antimicrobial peptides (AMP) are natural antibacterial agents of great interest for overcoming the problem of antibiotic resistance due to their peculiar mechanisms of action [1,3–10]. Among them, cathelicidins are a major family of AMPs of vertebrates that play a crucial role as components of innate immunity [11–13]. Among the cathelicidins of mammals, two interesting members are porcine PMAP-36 [7,14–16] and bovine BMAP-27 [17,18].

PMAP-36 is 36-mer amphipathic α-helical peptide that was originally isolated from porcine leukocytes (Ac-GRFRRLRKKTRKRLKKIGKVLKWIPPIVGSIPLGCG) [14]. This peptide has potent antimicrobial activity against a wide range of bacteria, including antibiotic-resistant strains [15]. PMAP-36 damages bacterial membranes through a carpet-like mechanism leading to cell lysis [19]. Several studies investigated structure-activity relationship aiming at identifying optimised shorter analogues of PMAP-36. The results obtained with truncated fragments such as PMAP-24 [20], PMAP-20 and PMAP-34 [21], PMAP-23 [22] and PMAP-18 [7] showed that only the longer peptides, which maintain helical structure, retain antimicrobial activity [23]. Recent data show that PMAP-36 fragments as short as 13 residues retain helicity and antimicrobial activity with MIC in the μM

* Corresponding author at: Department of Chemical Sciences, University of Padova, Padova, Italy
E-mail address: cristina.peggion@unipd.it (C. Peggion).

https://doi.org/10.1016/j.bioorg.2025.108715
Received 16 April 2025; Received in revised form 19 June 2025; Accepted 29 June 2025
Available online 30 June 2025

range and a broad spectrum of action [24]. The most interesting peptides identified in that study were PMAP(12–24) (Ac-KRLKKIGKVLKWI-NH_2) and PMAP-[U]21(12–24), which contains the non-proteinogenic amino acid Aib (U) [25–27]. However, despite their maintained potent antibacterial activity and low haemolysis, these two analogues proved to be still susceptible to proteolytic degradation and potential cytotoxic [24].

BMAP-27 is a cathelicidin-derived peptide isolated from bovine neutrophils [17]. This peptide also exhibits broad-spectrum antimicrobial activity against Gram-positive and Gram-negative bacteria, as well as antifungal properties. BMAP-27 is proposed to act through a toroidal pore mechanism by disrupting bacterial membranes [18]. BMAP-27 (GRFKRFRKKFKKLFKKLSPVIPLLPHR-NH_2) is a 27-mer antimicrobial peptide structured in an amphipathic α-helix [28]. The fragment BMAP (1–18) (GRFKRFRKKFKKLFKKLS-NH_2) retains remarkable antimicrobial potency both against Gram-positive and Gram-negative bacteria, but was inactive in vivo in a model of murine pneumonia due to its degradation by mice pulmonary proteases [29].

These peptide fragments displayed robust antimicrobial activity and were well tolerated by eukaryotic cells, suggesting a favorable compromise between antimicrobial effects and low cytotoxicity. This balance makes them a promising starting point for the development of more effective antimicrobial peptides. However, a common limitation shared by both native and synthetic AMPs is their susceptibility to proteolytic degradation. This is evident for both PMAP(12–24) and BMAP(1–18), which face significant challenges related to enzymatic breakdown, hindering their therapeutic potential. As such, optimizing peptide sequences to minimize cytotoxicity while enhancing resistance to proteolysis remains a critical challenge.

Several strate have been explored to improve the stability and selectivity of AMPs, including sequence modifications, cyclization, and the incorporation of non-natural amino acids [24,30,31]. One commonly employed approach is the use of *D*-amino acids, which are not susceptible to enzyme recognition, and are introduced strategically within peptide sequences to prevent proteolysis [32–34]. However, the targeted modification of specific residues may destabilize the overall three-dimensional structure of peptides, particularly since most natural AMPs adopt a right-handed α-helical conformation, determined by the presence of *L*-amino acids. Given that helicity is crucial for maintaining biological activity, a more advantageous approach involves inverting the configuration of all amino acids to achieve a left-handed helical structure, thus preserving the ability of the peptide to exert its biological effects [35,36]. *D*-enantiomeric peptides represent therefore a promising strategy to avoid in vivo degradation while maintaining antibacterial activity, as it has been done for BMAP(1–18) [29].

To investigate if this successful approach applied to BMAP(1–18) [29] may be extended also to PMAP derivatives, we selected PMAP (12–24) [37] [29] as the most promising candidate and synthesised its *D* and *L* enantiomers for direct comparison in terms of structure, resistance to protease degradation, antimicrobial activity and cytotoxicity. All-*D* and all-*L* BMAP(1–18) have also been synthesised, as a benchmark for PMAPs, but also to extend the characterisation of the two BMAP(1–18) enantiomers, which have great potential as antimicrobial molecules. Specific attention will be given to structure-activity relationship considerations.

2. Results and discussion

2.1. Design and synthesis of the peptides

The peptides designed for this study are shortened analogues of BMAP-27 and PMAP-36, specifically the 1–18 segment of the former and 12–24 segment of the latter, that retain the antimicrobial properties of the native peptides. Therefore, these sequences and their *D* enantiomers were selected to deepen the understanding of how structure relates to function. To preserve the helical conformation of the peptides while avoiding disruption of the amphipathic nature of the helices, key to their antimicrobial activity, we replaced all *L*-amino acids with *D*-amino acids [35]. This approach ensures that the overall charge and hydrophobicity conferred by the side chains of the amino acids remain unchanged, but the enantiomeric change is expected to confer resistance of the peptides to proteases.

The all-*D* and all-*L* enantiomers of both the peptides were synthetized. Peptides **a** and **b** are the two enantiomers derived from PMAP-36, while peptides **c** and **d** are the two enantiomers derived from BMAP-27.

The designed peptides (**a**-**d**) are amidated at the C-terminus and acetylated at the N-terminus. The strategy of capping the N-terminus of peptides with different acyl groups is commonly used to increase the proteolytic stability of short peptides in vitro and in vivo [38]. All peptides were successfully synthesised in high purity using the Solid Phase Peptide Synthesis method [39], and their masses were confirmed through ESI-MS, supporting the reliability of the synthesised constructs (Table 1).

The shortened analogues, PMAP(12–24) and BMAP(1–18), reduced both the time and cost of synthesis with respect to the longer native cathelicidins and were expected to not compromise the helical structure of the original peptides or their antimicrobial activity, that was however assessed as follows.

2.2. Conformational analysis

Circular dichroism (CD) spectroscopy was employed to investigate the secondary structures of the synthesised peptides, essential to elucidate their mechanism of antimicrobial action. Measurements were carried out in phosphate buffer (PB, pH = 7,0), 100 mM sodium dodecyl sulfate (SDS) and 2,2,2-trifluoroethanol (TFE). Since the mechanism of action of these peptides involves membrane disruption through interactions with lipids, SDS was selected as a first approximation of the bacterial membrane amphipathic environment and provided insight into the behaviour of peptides under these conditions. TFE was instead chosen as it promotes the formation of helical structures in peptides [40–42].

In aqueous solution, all peptides exhibited a characteristic maximum around 200 nm, negative for the *L*-enantiomers and positive for the *D*-enantiomers, which is indicative of unordered or random coil structures (Fig. 1A and B) [43]. This observation is consistent with previous studies on membranolytic antimicrobial peptides, which commonly adopt disordered structures in aqueous environments before interacting with membranes [44].

Conversely, in membrane-mimetic environments such as SDS (Fig. 1A, light and dark green), peptides **a** and **c** displayed the typical CD spectral signature of helical structures, characterized by three bands: two negative maxima at 222 nm and at around 206–208 nm, along with a positive maximum around 190 nm. These features correspond to the parallel component of the $\pi \rightarrow \pi^*$ transition, the $n \rightarrow \pi^*$ transition, and the parallel component of the $\pi \rightarrow \pi^*$ transition, respectively. The spectra of peptides **b** and **d** were mirror images of their *L*-enantiomer counterparts, indicating the formation of left-handed helices. The left-handed helical structure of the *D*-enantiomers (peptides **b** and **d**) supports the reasonable assumption that the *D*-enantiomers likely follow a similar mechanism of action as their corresponding *L*-enantiomers. This also aligns with the proposed mechanism of action for these peptides, where helical structures facilitate membrane disruption through perturbation or insertion into the membrane [44,45].

In the presence of SDS, the maximum at 220 nm was not well defined for PMAP-36 analogues (**a** and **b**) (Fig. 1A), resembling a shoulder rather than a distinct peak, and the 206 nm band associated with the $n \rightarrow \pi^*$ transition was slightly shifted from the ideal value of 208 nm. This suggests a deviation from the canonical α-helix conformation. Furthermore, the ratio of the molar ellipticity at 222 nm to that at 206 nm, R ($[\Theta]_{222}/[\Theta]_{206}$), was significantly lower than the ideal value close to 1 as for a typical α-helix. The values around 0.6, approaching the range

Table 1
List of the synthetized peptides and of their physico-chemical properties.

	Name	Peptide sequence	$[M+H]^+_{calcd}$	$[M+H]^+_{exp}$	Purity %	t_R * (min)
	PMAP-36	H-GRFRRLRKKTRKRLKKIGKVLKWIPPIVGSIPLGCG-NH_2				
a	*L*-PMAP(12–24)	Ac-KRLKKIGKVLKWI-NH_2	1651.1	1651.1	96	13.5
b	*D*-PMAP(12–24)	Ac-krlkkigkvlkwi-NH_2	1651.1	1651.1	99	12.4
	BMAP-27	H-GRFKRFRKKFKKLFKKLSPVIPLLHLG-NH_2				
c	*L*-BMAP(1–18)	Ac-GRFKRFRKKFKKLFKKLS-NH_2	2383.5	2383.1	95	14.4
d	*D*-BMAP(1–18)	Ac-grfkrfrkkfkklfkkls-NH_2	2383.5	2383.1	96	14.7

* Retention time refers to 10–40 %%B (CH_3CN/H_2O, 9:1) over 30 min gradient for **a** and **b** and 15–45 %B over 30 min gradient for **c** and **d**. Binary elution system A: 0.05 % TFA (2,2,2-Trifluoroacetic acid) in CH_3CN/H_2O (1:9 *v*/v) and B: 0.05 % TFA in CH_3CN/H_2O (9:1 v/v). Phenomenex Luna C18 column (4.6 × 250 mm, 5 μ, 100 Å).

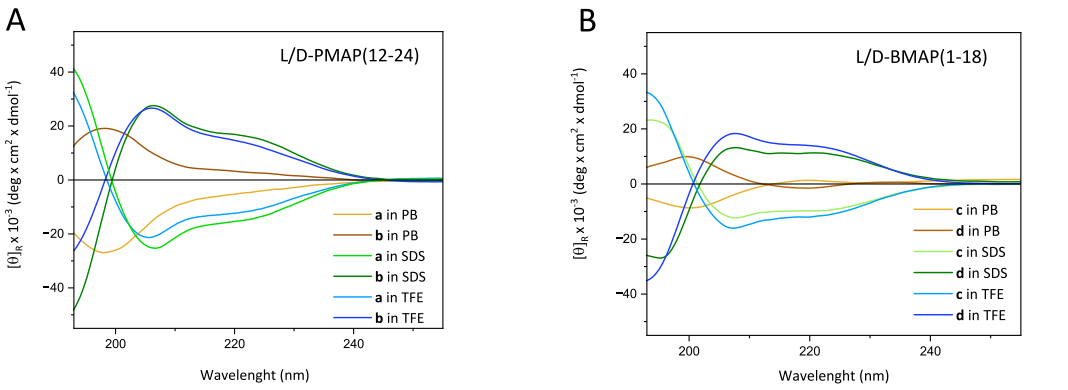

	SDS	TFE
Peptide	R ($[\vartheta]_{222}/[\vartheta]_{206}$)	R ($[\vartheta]_{222}/[\vartheta]_{206}$)
a	0.59	0.54
b	0.59	0.51

	SDS	TFE
Peptide	R ($[\vartheta]_{222}/[\vartheta]_{208}$)	R ($[\vartheta]_{222}/[\vartheta]_{208}$)
c	0.78	0.71
d	0.82	0.73

Fig. 1. CD spectra and R($[\Theta]_{222}/[\Theta]_{206-208}$) values for (**A**): *L*-PMAP(12–24) (**a**) and *D*-PMAP(12–24) (**b**). (**B**): *L*-BMAP(12–24) (**c**) and *D*-BMAP(12–24) (**d**). The spectra were taken in PB (yellow/brown), SDS (light and dark green) and TFE (light and dark blue), at 25 °C. (For interpretation of the references to colour in this figure legend, the reader is referred to the web version of this article.)

(0.4–0.5) characteristic of 3_{10}-helical peptides [46–49], suggested a mixed 3_{10}−/α-helical conformation. In contrast, the R($[\Theta]_{222}/[\Theta]_{208}$) ratio for the two BMAP-27 analogues (**c** and **d**) (Fig. 1B) was approximately 0.7–0.8, demonstrating a predominant α-helical character [50], in agreement with previous studies on BMAP18 [51]. The results obtained in TFE (Fig. 1A and B, light and dark blue) were very similar to those observed in SDS, suggesting a complete structuration already in the presence of SDS (and hypothetically also in the presence of biological membrane). Moreover, spectra measured in TFE corroborated a mixed 3_{10}−/α-helical structuration for PMAP(12–24) and the prevalence of α-helices for BMAP(1–18). The conformational analysis also revealed subtle differences between the two peptide groups. Specifically, the PMAP-36 analogues (peptides **a** and **b**) are likely to adopt mixed α−/3_{10}-helical conformation, with the ratio of the molar ellipticity at 222 nm and 206 nm favouring the 3_{10}-helix, both in SDS and in TFE [47]. On the other hand, the BMAP-27 analogues (peptides **c** and **d**) exhibit a greater contribution of α-helix in SDS and in TFE, with R values suggesting a preference for the α-helix. This observation is consistent with previous findings that 3_{10}-helical structures are more common in short peptides rather than in longer ones [46,52].

Finally, the relative intensity of the CD bands for the two peptide groups indicates that PMAP has a greater helical content than BMAP. This increased helicity may enhance the ability of PMAP to interact with lipid bilayers, suggesting that PMAP(12–24) is better suited to interfere with bacterial membranes.

To obtain a deeper view of the conformational preferences of the peptides, 2D-NMR analysis was performed in TFE-d2 solution. The NMR spectra of **a** was already reported in a previous work [24]. As an explicative example the spectra of peptide **c**, BMAP(1–18) are here reported.

2D TOCSY and NOESY NMR spectra were recorded in d_2-TFE, and complete assignment of proton resonances was established for peptide **c**, using the procedure proposed by Wuthrich [53]. The Cα signals were clearly identified from the TOCSY spectrum, with the full assignment provided in the Supporting Information. In the NOESY spectrum (Fig. 2A), most of the αCH(i) → NH(i + 1) cross-peaks are readily visible, confirming the presence of well-defined sequential connectivities [53–55]. More importantly, all the NH(i) → NH(i + 1) sequential NOE cross-peaks are clearly observed, supporting the presence of a stable helical conformation (Fig. 2B). These sequential NOEs are strong indicators of a defined and consistent secondary structure, typical of α-helices.

Some long-range NOE cross-peaks were also observed in the NOESY spectrum. Specifically, the presence of the αCH(i) → NH(i + 2) cross-peak between Lys8 and Phe10, as well as the αCH(i) → NH(i + 3) cross-peaks between Phe10 and Leu13 and Lys11 and Phe14 (Fig. 2A), are indicative of a mixed α/3_{10} helical conformation [55]. These long-range interactions are characteristic of peptides adopting a hybrid secondary structure, supporting the conclusion that both α- and 3_{10}-helical elements are present in the overall peptide conformation. In the NMR spectra of the other peptides similar NOE cross-peaks were observed, particularly αCH(i) → NH(i + 3), which is indicative of a helical structure, though these data do not distinguish between different types of helices (data not shown).

The NMR analysis corroborated the findings from circular dichroism (CD) measurements, confirming that peptide **c** adopts both 3_{10}- and

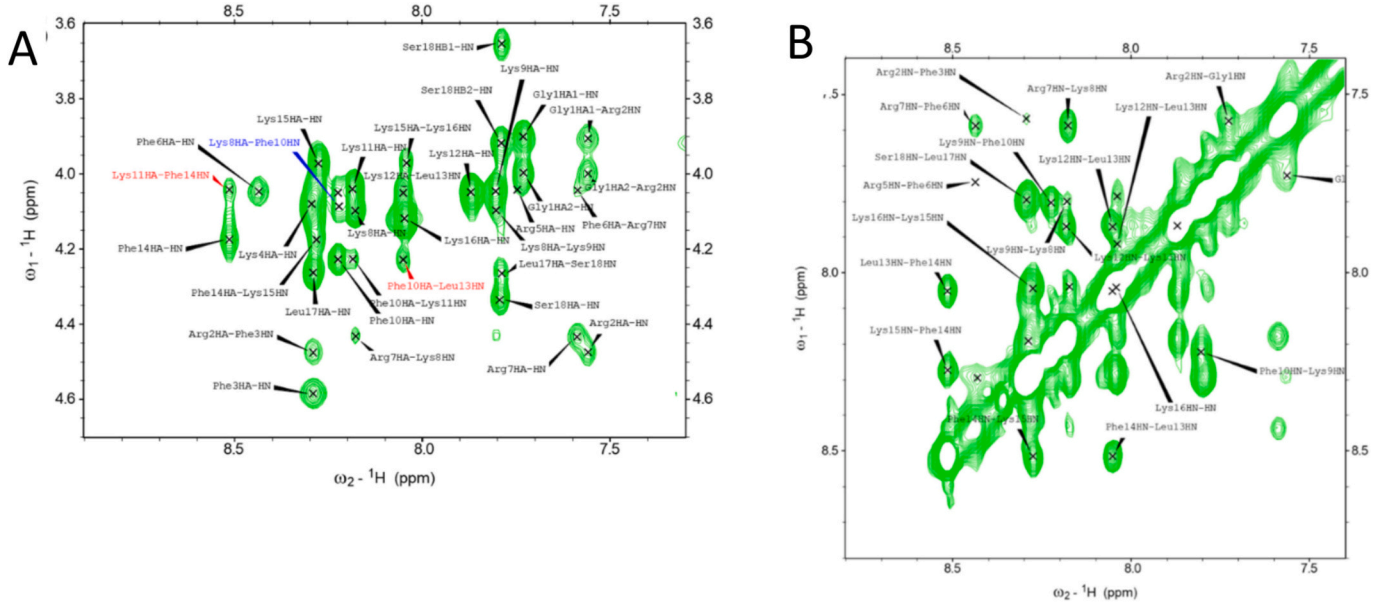

Fig. 2. Regions of the NOESY spectrum of peptide **c**, *L*-BMAP(1–18) (600 MHz, TFE d2, 308 K). (**A**) Fingerprint region where the αCH(i) → NH(i + 2) and αCH(i) → NH(i + 3) cross-peaks are highlighted in blue and red, respectively. (**B**) NH(i) → NH(i + 1) region of the NOESY spectrum. (For interpretation of the references to colour in this figure legend, the reader is referred to the web version of this article.)

α-helices in TFE solution. Overall, for all peptides, the helical structure observed in TFE, as indicated by the CD results, was further validated by NMR analysis.

2.3. Proteolytic stability

The stability of antimicrobial peptides against proteolytic degradation is a major challenge in their development as potential peptide drugs. In this study, we investigated the stability of the synthetic peptides when exposed to trypsin [56,57] and human serum. After incubation with either enzyme or serum, the integrity of the peptides was monitored by HPLC. Proteolytic degradation is reported as a function of time (Fig. 3) [56,57].

As shown in Fig. 3, both peptides **a** and **c**, the *L*-enantiomers, were readily degraded by trypsin and serum. In trypsin solution, the degradation of the *L*-enantiomers **a** and **c** started immediately after the addition of protease, with a loss of 50 % and 95 %, respectively, at the first time point (10 min). Peptide **c** was completely degraded after 15 min, whereas peptide **a** was slightly more resistant, with complete degradation occurring within 30 min. The degradation products of peptide **c** were not detectable in the HPLC chromatograms (Supporting Information). In human serum (Fig. 3B), degradation products of peptides **a** and **c** were detected after 15 min, while complete degradation occurred in the first few hours, with 20 % of PMAP-36 derivative **a** still visible after 6 h. On the other hand, the *D*-enantiomers, peptides **b** and **d**, as expected, were not degraded both in the presence of trypsin and serum (Fig. 3), with chromatograms remaining unchanged throughout the 24-h period of analysis (Supporting Information).

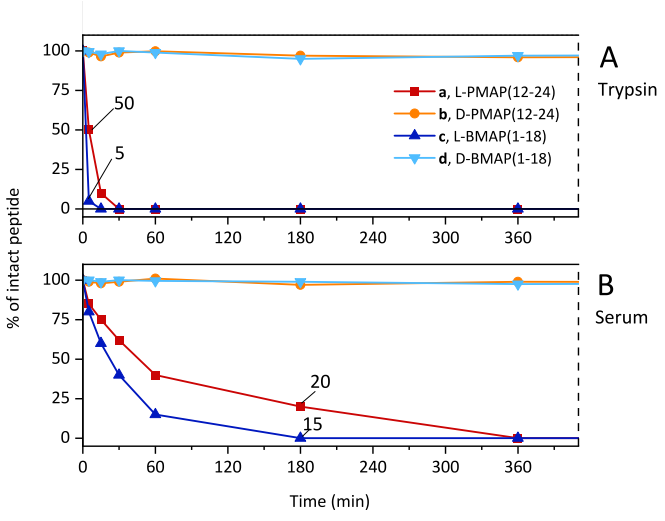

Fig. 3. Proteolytic degradation of the peptides **a**-**d** in trypsin (A) and human serum (B), represented as the percentage of intact peptide over time calculated as the HPLC-peak area. (An example of the HPLC profiles with labelled peaks corresponding to hydrolysis products is reported in the Supporting Information, Fig. S8).

Peptides **a** and **c** both underwent rapid degradation upon exposure to trypsin. This immediate breakdown suggests the formation of small fragments that are likely undetectable by HPLC, which aligns with the known mechanism of action of trypsin [56,57]. Trypsin is a highly specific and efficient protease that cleaves peptide bonds on the carboxyl side of lysine and arginine residues, that constitute more than 50 % of the amino acid residues of peptide **c**. The degradation of both the peptides was slower in serum. Discrepancy between the observations in trypsin and serum could be due to different ratio between peptides and enzyme, given that serum contains a complex mixture of enzymes that cannot be accurately measured. Moreover, the abundance of proteins in serum offers to the peptides several possible interactions that may partially shield them from the proteases.

The potential advantages of using *D*-peptides are therefore evident in applications where resistance to proteolytic degradation is critical for bioavailability and efficacy.

2.4. Membranolytic properties

The antimicrobial peptides PMAP-36 and BMAP-27 exert their activity through a membranolytic mode of action, disrupting integrity of bacterial membranes [44,58,59], although through different mechanisms. To investigate the interactions among the peptides synthesised in this study and the biological membranes, a carboxyfluorescein (CF) leakage assay was conducted using DOPE/POPG (7:3) liposomes, which

are artificial bilayers that mimic the lipid composition of Gram-negative bacterial membranes. Increasing concentrations of the peptides were added to the liposomes, and fluorescence measurements were taken after incubation. Trichogin GAIV, a peptide with well-established membranolytic activity [15,60], was used as a benchmark.

The behaviour of the PMAP analogues was comparable to that of the membranolytic control, confirming a marked ability of shorter PMAPs derivatives to interact with- and permeabilize bacterial membranes (Fig. 4) as reported for another derivative consisting of the first 24 N-terminal residues PMAP36 [19] instead of the central 12–24 residues used in this study. In contrast, the BMAP-27 analogues, showed a lower ability to damage liposomes inducing CF leakage. The moderate fluoresceine leakage induced by shorter BMAP-27 derivatives has already been reported and does exclude that BMAP-27 derivatives can affect the bacterial membrane. In fact, BMAP27(1–18) can induce small discontinuities in the bacterial envelope whose reduces size impairs large molecules such as calcein to pass through and to exit the liposomes. On the other hand, the damages exerted by BMAP27(1–18) to the bacterial envelope are still relevant from a functional point of view, since they end in the depolarization [61] or the permeabilization [50] of the bacterial membranes, which becomes visible using small dyes like the propidium iodide.

The two sets of peptides, PMAP-36 analogues (peptides **a** and **b**) and BMAP-27 analogues (peptides **c** and **d**), likely exhibited differences in interaction with the target membranes, evaluated by using DOPE/POPG liposomes. Peptides **a** and **b**, which independently of their chirality, exhibited potent membrane disrupting behaviour comparable to that of the full length PMAP-36 [19,20] but also with the positive control Trichogin GAIV, are likely to act by a mechanism that does not require spanning of the lipid bilayer, but rather by a carpet-like action disrupting membrane integrity, as it had been widely demonstrated in the literature [25,62–64]. In contrast, our data on the BMAP-27 analogues (peptides **c** and **d**) indicate lower, but still appreciable membrane permeabilization on a model of Gram-negative membranes, confirming and complementing previous analyses on BMAP-18 performed on the Gram-positive *S. aureus* [51]. It is likely that the shortened peptides, with respect to their native molecules, are unable to organize into aggregates spanning the bilayer [65,66], resulting in less efficient membranolytic behaviour. The differences observed for the two peptide groups may instead be due to differences in helix content as observed in CD analysis, where PMAP(12–24) have a higher helix content than BMAP(1–18).

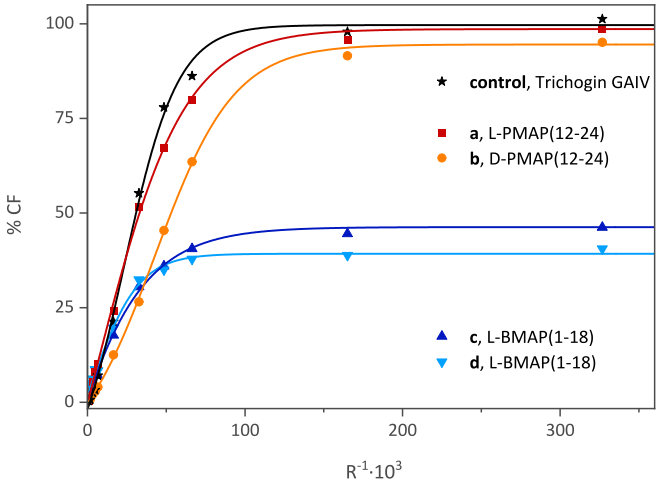

Fig. 4. Peptide-induced CF leakage at 20 min for different ratios R^{-1} = [peptide]/[lipid] in DOPE/POPG 7:3 vesicles.

2.5. Antibacterial activity and cytotoxicity

The antimicrobial activity of the four derivatives was evaluated by determining the minimum inhibitory concentration (MIC) and minimum inhibitory concentration (MBC) against a panel of Gram-positive *(S. aureus, S. epidermidis)* and Gram-negative (*A. baumannii, K. pneumoniae, P. aeruginosa*) bacterial strains (Table 2). The conventional antibiotics tobramycin and rifampicin were also tested to make a comparison, as well as the lipopeptide lytic last-resort antibiotic colistin (Table 3S).

The peptides showed potent, broad-spectrum antimicrobial activity, inhibiting all strains with MIC values ranging from 1 to 16 μM, often comparable with those of reference antibiotics (Table 3S). The only exception was the peptide **a,** which was ineffective against *S. aureus* (MIC>64 μM), as previously reported with the same strains for compound **a** [24]. Interestingly, these shortened peptides experienced only a partial a reduction of their antimicrobial efficacy with respect to their full-length relatives. E.g., the peptide PMAP-36 (1–34) had MIC = 1 μM toward the same ATCC strains of *S. aureus*, *E. coli* and *P. aeruginosa* used in this work [21]. Similarly, previous studies on the full-length BMAP-27 [67] reported MIC_{90} > 64 μg/mL (corresponding to >20 μM) against a panel of clinically isolated *S. aureus* strains and an MIC_{90} = 16 μg/mL (corresponding to 5 μM) against a panel of clinical isolates of *P. aeruginosa.* Notably, both *D*-form peptides **b** and **d** displayed antimicrobial activity comparable with- or, in some cases, greater than their *L*-counterparts. Specifically, peptide **b** demonstrated higher antibacterial activity than its enantiomer against *S. aureus* (MIC = 16 μM vs >64 μM), while *D*-peptide **d** exhibited two-fold decrease in MIC across all the tested strains compared to its *L*-isomer. PMAP derivatives were more active than BMAP derivatives against Gram-negative strains *A. baumannii*, *K. pneumoniae*, and *P. aeruginosa.* In contrast, BMAP derivatives were more effective against gram-positive *S. aureus* and *S. epidermidis.* Interestingly, this general trend was observed when comparing the *D*-enantiomers. These results suggest possible clinical applications of these peptides. Both the *L*- and *D*- isomers of BMAP (1–18) in previous experimentation on a panel of *P. aeruginosa* clinical isolates from cystic fibrosis displayed MIC values mainly in the range of 8–16 μg/mL (corresponding to 3,5–7 mM) [17,29]. So, given the higher antimicrobial effect of both the PMAPs toward this pathogen with respect to the BMAPs, it would be interesting to investigate the potential also of PMAPs to target *P. aeruginosa* in relevant clinical context like cystic fibrosis or other opportunistic infections by this pathogen.

The differences in the antibacterial effects between enantiomers of the same peptides are moderate but still worthy of analysis (Table 2). This trend had been already observed for the enantiomers of BMAP-18 analysing panels of both *P. aeruginosa* and *S. aureus* [29], in line with data collected in the current study. A possible explanation for the slightly enhanced antimicrobial activity of *D*-enantiomers is that peptides containing *L*-amino acids may undergo partial degradation by bacterial enzymes during incubation. On the other hand, peptides containing *D*-amino acid were resistant to such enzymatic degradation, making them more effective. *D*-enantiomers may therefore offer advantages in specific contexts, potentially providing greater stability against proteolytic degradation and improving the overall therapeutic potential of the peptides.

It is worth noting that the MBC values often matched the MIC values and, only in a few cases, were twice the MIC. This confirms the bactericidal nature of all derivatives, which is desirable for antimicrobial compound as allows them to eradicate bacterial pathogens and not only to limit their replication. These features of all the considered peptides are also informative and confirmative for their mode of action. The near-complete overlap between MIC and MBC values is in line with the typical behaviour of strong membrane-permeabilizing antimicrobial agents [68].

The effects of PMAP-36 and BMAP-27 derivatives, along with their *D*-enantiomers, were evaluated on eukaryotic cells. To assess cell

Table 2
Minimum inhibitory and bactericidal concentrations (MIC and MBC, μM) of BMAP- and PMAP-derivatives toward reference strains representative of pathogens of clinical concern.

	E. coli		*S. aureus*		*A. Baumanni*		*K. pneumoniae*		*P. aeruginosa*		*S. epidermidis*	
	ATCC 25922		ATCC 25923		ATCC 19606		ATCC 700603		ATCC 27853		ATCC 12228	
Peptide	**MIC**	MBC	**MIC**	MBC	**MIC**	MBC	**MIC**	MBC	**MIC**	MBC	**MIC**	MBC
a	4	4	>64	>64	2	2	4	4	8	8	4	4
b	2	2	16	32	2	2	4	4	4	4	4	4
c	8	16	16	16	8	16	16	16	16	32	2	2
d	4	8	8	8	8	8	8	16	8	16	1	1

viability in the presence of the peptides, the MTT metabolic assay was performed on mouse embryonic fibroblast 3 T3 cell line, incubated with increasing concentrations of each compound (Fig. 5). *L*-enantiomers of both peptides did not cause a significant reduction in cell viability after 24 h of incubation, at concentrations up to 16 μM. However, at 32 μM, both the **a** and **c** peptides resulted in approximately a 40 % decrease in cell viability.

The *D*-enantiomer of PMAP(12–24) exhibited a similar behaviour, showing no significative increase in cytotoxicity compared to its all-*L* enantiomer. In contrast, the *D*-enantiomer of BMAP(1–18) at 16 μM reduced cell viability, with levels falling below 50 % at higher peptide concentrations. Notably, the *D*-form of BMAP(1–18) appeared more cytotoxic than its *L*-counterpart, though these concentrations (16 and 32 μM) are generally higher than those required for bactericidal activity. These findings align with previous data on BMAP(1–18) [27]. This behaviour might be attributed to the greater stability of *D*-enantiomers, which protects them from proteolytic degradation in both bacterial and eukaryotic cells but possibly enhancing cytotoxic phenomena. However, overall, the increased activity of the *D*-enantiomers was accompanied by a slight decrease in biocompatibility with 3 T3 fibroblasts only in the case of BMAP(1–18) and not PMAP(12–24), whose *D*-enantiomer did not display the dramatic gap in tolerability by eukaryotic cells that was observed comparing *L*- and *D*- BMAP(1–18).

3. Conclusions

This study provided insights into how the chirality of amino acids in cathelicidin peptides PMAP(12–24) and BMAP(1–18) affects antimicrobial activity, stability profiles, and how structural differences between the peptides influence activity and cytotoxicity.

Although both the *L*- and *D*-forms of these peptides adopt helical structures in membrane-mimetic environments, subtle differences were observed between their PMAP-36 and BMAP-27 derivatives, which could be correlated with differences in their spectrum of activity and mechanism of action. PMAP-36 analogues were more prone to adopting mixed $\alpha/3_{10}$-helical conformations, a behaviour commonly observed in short natural antimicrobial peptides. At the same time, these derivatives effectively disrupted artificial membranes, suggesting a carpet-like mechanism. This enhanced membrane-disrupting ability correlated with superior antimicrobial potency, particularly against Gram-negative bacteria such as *A. baumannii*, *K. pneumoniae* and *P. aeruginosa*. Conversely, BMAP-27 analogues favoured a more pronounced α-helical structure and destabilised membranes possibly by forming smaller pores. Their antimicrobial activity was mainly directed against Gram-positive bacteria.

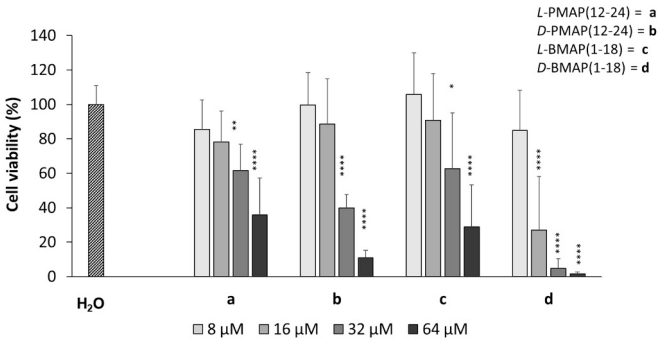

Fig. 5. Effects of PMAP (12–24) and BMAP(1–18) derivatives on the viability of 3 T3 cell line. MTT assay on 3 T3 cells after treatment with different concentration of peptides. Cell viability was measured (as absorbance at 570 nm) 24 h after treatment with different concentrations of peptide. Samples treated with water instead of peptides were set as 100 % of viability (H_2O). Data are the mean ± standard deviation of five independent experiments in internal triplicate ($n = 15$). One-way ANOVA and Tukey's multiple comparisons test. *$p \leq$ 0,05; ** p ≤ 0,01; *** p ≤ 0,001; ****$p <$ 0,0001 vs Untreated control (H_2O).

The *D*-enantiomers proved to be advantageous in terms of proteolytic stability, not only against trypsin but also in a physiological environment, such as human serum. Another benefit of using *D*-enantiomers was their enhanced antibacterial activity, likely due to increased resistance to bacterial proteolytic enzymes. However, *D*-enantiomer of BMAP (1–18) appeared to be slightly more cytotoxic than their *L*-form counterpart, raising issues that require further investigation. Nonetheless, they remained biocompatible at concentrations effective against bacteria.

In conclusion, *D*-enantiomeric analogues of PMAP-36 and BMAP-27 peptides exhibit a promising combination of antimicrobial activity, proteolytic stability, and low cytotoxicity. In particular, *D*-PMAP (12–24) showed the most favorable properties for further optimisation to enhance its bioactivity, making it a strong candidate for therapeutic development.

4. Experimental

4.1. Peptide synthesis

All the peptides were synthetized by solid phase peptide synthesis with an automatic *Syro Wave* synthesizer (Biotage, Uppsala, Sweden), using standard Fmoc-chemistry strategy [37,62]. For all the peptides Fmoc Rink Amide AM resin (loading 0.64 mmol/g) was used as the solid support. The amino acids of the *L*-peptides were activated with 3 eq. of Oxyma Pure (Ethyl cyano(hydroxyimino)acetate)/DIC (*N,N*′-Diisopropylcarbodiimide), whereas the ones of the *D*-peptides were activated with 3 eq. of HBTU (*N,N,N*′,*N*′-Tetramethyl-O-(1H-benzotriazol-1-yl) uronium hexafluorophosphate)/HOBt (Hydroxybenzotriazole) and 6 eq. of DIPEA (N,N-Diisopropylethylamine). The coupling was performed with 3 eq. of activated protected amino acid (1 h) in DMF (*N,N*-dimethylformamide). Deprotection of the Fmoc group was carried out with a 20 % piperidine solution in *N,N*-dimethylformamide (2 × 10 min). The cleavage of the peptides from the resin was performed with a TFA/H_2O/TIS (Triisopropylsilane) mixture in a 95:2.5:2.5 ratio. The recovery of the crude peptide was achieved by precipitating the filtrated peptide solution in diethyl ether, centrifuging (10 min at 5500 rpm x3) and drying the solid in a desiccator under reduced pressure.

The peptides were purified with an Isolera Prime chromatographer (Biotage, Uppsala, Sweden) using a Biotage SFAR Bio C18 (100 Å, 12 g) cartridge and a binary elution system (A: H_2O + 0.05 % TFA, B: CH_3CN/H_2O 9:1 *v*/v; gradient from 10 to 45 %B in 50 min). The purified

peptides were freeze-dried from 0.1 M HCl to constant weight and characterized by analytical HPLC and ESI-MS. For the HPLC a *Phenomenex Luna C18* column (4.6 × 250 mm, 5 μ, 100 Å) was used coupled to a VWR HITACHI Chromaster instrument with a spectrophotometric detection at λ = 214 nm and λ = 280 nm. The binary elution system used was A: 0.05 % TFA in CH_3CN/H_2O (1:9 *v*/v) and B: 0.05 % TFA in CH_3CN/H_2O (9:1 v/v). ESI-MS was performed using an Agilent technologies 1260 Infinity II instrument equipped with an Agilent technologies quadrupole LC–MS 6130. All the peptides had a purity >95 % and were stored at −20 °C.

4.2. Circular dichroism

The circular dichroism spectra of 2×10^{-4} M solutions of the peptides in TFE (99.9 % Acros Organics, Geel, Belgium), PB (phosphate buffer) and 100 mM SDS (the final molar peptide-to-lipid ratio is 1:300) were recorded at room temperature on a *J-1500 spectropolarimeter* (Jasco, Tokyo, Japan) with a fused quartz cell of 0.02 cm pathlength (Hellma, Mühlheim, Germany). The values are expressed in total molar ellipticity ($[\theta]_R$, deg. × cm^2 × $dmol^{-1}$).

4.3. NMR

The monodimensional and correlated spectroscopy (COSY)/total correlation spectroscopy (TOCSY) and NOESY 2D NMR spectra of the selected analogues were obtained at 308 K by the use of a Bruker AVANCENEO-600 spectrometer from an about 1.5 mM concentration sample dissolved in approximately 700 μL of TFE,d2 solution. Suppression of the solvent signal was achieved by the use of an excitation sculpting program [69]. All homonuclear spectra were acquired by collecting 512 experiments, each one consisting of 64–80 scans and 2 K data points. The spin systems of the coded amino acid residues were identified using standard double-quantum filtered-COSY [70] and clean TOCSY [71] spectra. In the latter case, the spin-lock pulse sequence was 70 ms long. NOESY experiments were utilized for sequence-specific assignments [53]. To avoid the problem of spin diffusion, the build-up curve of the volumes of the NOE cross peaks as a function of the mixing time (50–500 ms) was obtained first (data not shown). The mixing time of the NOESY experiment used for interproton distance determination was 150 ms (i.e., in the linear part of the NOE build-up curve).

4.4. Proteolytic stability

The proteolytic stability of the synthetized peptides was tested using trypsin (Sigma-Aldrich) and human serum (Sigma-Aldrich [72]). When using trypsin, the samples were prepared in a total volume of 1 mL, diluting a 5 mg/mL solution of the peptides in DMSO and a 1 mg/mL of enzyme in water with Tris·HCl (50 mM, pH 7.8) up to 0.25 mg/mL and 0.0025 mg/mL, respectively. The samples were incubated for 24 h at 37 °C and at selected timepoints 50 μL of the solution were withdrawn and added to 200 μL of EtOH at 0 °C (15 min). The supernatant of the solution was analysed by RP-HPLC. A sample without the enzyme was used as control. All the degradation experiments were executed in triplicates.

When using human serum the measure and control samples were prepared by adding 40 μL of a 5 mg/mL solution of the peptide in DMSO to 1 mL and 1.25 mL of 25 mM HEPES, 2-[4-(2-hydroxyethyl)piperazin-1-yl]ethanesulfonic acid, buffer (pH 7.2), respectively. Then to start the measurement 250 μL of human serum (20 %) were added to the measure sample. The samples were incubated for 24 h at 37 °C and at selected timepoints 100 μL of the solution were withdrawn, added to 200 μL of deionized water and subjected to 3 cycles of 5 min at 100 °C and then 5 min at 0 °C.

4.5. Leakage from liposomes

4.5.1. Liposome preparation

DOPE (1,2-dioleoyl-sn-glycero-3-phosphoethanolamine) and POPG (1-Palmitoyl-2-oleoyl-sn-glycero-3-phosphoglycerol) (Avanti Polar Lipids) were dissolved in CH_2Cl_2 in a ratio of 7:3. Then CH_2Cl_2 was removed under a flow of N_2, an excess of a 40 mM carboxyfluorescein solution in HEPES 5 mM was added and the solution was left in the dark for the night. The liposomes were purified by exclusion size column chromatography using Sephadex as the solid phase and a 100 mM NaCl solution in HEPES 5 mM as the eluent. The purified liposomes were stored in 0.06 mM solutions of the eluent at 0 °C.

4.5.2. Leakage test

A LS50B Luminescence Spectrometer (Perkin Elmer) with a $\lambda_{excitation}$ of 488 nm and $\lambda_{emission}$ of 520 nm (excitation and emission slits of 5.0 and 7.5 nm, respectively) was used to record the fluorescence of the solutions of peptide-liposomes. The samples were prepared by adding increasing amounts of peptide to 0.06 mM liposome solutions in 100 mM NaCl/5 mM HEPES (peptide concentration range from 4×10^{-5} mM to 3×10^{-2} mM) and incubating them for 20 min (F_t). Then 50 μL of a 10 % *Triton* solution was added to the samples and the fluorescence was recorded again (F_{TOT}). Trichogin GA IV peptide was used as a control.

4.6. Cell experiments

4.6.1. Bacterial culture

The bacterial strains used *were Escherichia coli* ATCC 25922*, Staphylococcus aureus* ATCC 25923*, Klebsiella pneumoniae* ATCC 700603*, Acinetobacter baumannii* ATCC 19606*, Pseudomonas aeruginosa* ATCC 27853 *and Staphylococcus epidermidis* ATCC 12228, purchased from American Type Culture Collection (ATCC) (Manassas, Virginia, USA). Bacterial culture was e grown overnight (o/n) at 37 °C in complete Müller-Hinton broth (MHB, Difco) with shaking (130 rpm). The day after, the overnight bacterial cultures were diluted 1:30 in fresh MHB and incubated at 37 °C with shaking (130 rpm) for approximately 2 h (mid-log phase) until reaching an optical density (OD) at 600 nm (OD_{600}) ≈ 0.3.

4.6.2. Minimum inhibitory and bactericidal concentration (MIC and MBC) assay

Peptides diluted in MHB to a concentration of 128 μM were added to the first column of wells of a 96-well round-bottom microtiter plate (Sarstedt, Milan, Italy) and two-fold serially diluted in a final volume of 50 μL MHB. Then, mid-log bacterial cultures ($OD_{600} \approx 0.3$) were diluted to 5×10^5 colony-forming units (CFU)/mL in MHB and 50 μL of this bacterial suspension was added to each well. Halving in this way, the final bacterial concentration to 2.5×10^5 CFU/mL and the peptide concentration in the wells in a final volume of 100 μL (final bacteria load was 2.5×10^4 CFU/well). The same number of bacteria in untreated MHB was used as a control for bacterial growth. MHB only (100 μL) was used as a negative control to check the sterility of the medium. The plate was sealed with parafilm to minimize evaporation and incubated overnight at 37 °C (approximately 18 h). MIC was determined by visual inspection at the end of incubation as the first clear well.

After having checked the MIC, to calculate the MBC, 25 μL from all the clear wells were taken after pipetting, then plated on agarized MH medium. Plates were incubated o/n at 37 °C and the day after viable colonies were counted. The MBC was the conditions killing 99.9 % of the initial bacterial inoculum.

Data are reported as the mode of independent experiments repeated three times or four times in case of uncertain values.

4.6.3. Cytotoxicity assay on human cells

Cell viability was assessed using the tetrazolium salt (MTT) assay as previously reported [73]. NIH/3 T3 murine fibroblasts (ATCC CRL-

1658) were cultured at 37 °C with 5 % CO_2 until they reached approximately 80 % confluence in a T-25 flask (Sarstedt) containing 5 mL of Dulbecco's Modified Eagle's Medium (DMEM, Sigma-Aldrich), supplemented with 100 U/mL penicillin (Sigma), 100 µg/mL streptomycin (Sigma), 2 mM L-glutamine, and 10 % (*v*/v) fetal bovine serum (EuroClone). Upon reaching sub-confluence, cells were detached by incubating with 2 mL of trypsin solution (500 mg/L trypsin, 370 mg/L EDTA, EuroClone SpA) for 5 min at 37 °C. Trypsin was then neutralized with 4 mL of complete DMEM. Cells were counted using a Burker-Türk chamber in the presence of 1 mg/mL trypan blue to confirm the absence of non-viable cells. The suspension was then diluted in complete DMEM to achieve a final concentration of 5×10^4 cells/mL. Subsequently, 100 µL of this suspension was seeded into 96-well flat-bottom microtiter plates (Sarstedt) and incubated overnight at 37 °C with 5 % CO_2. The following day, the spent medium was removed and replaced with 100 µL of peptide solutions prepared at the desired concentrations in DMEM. Untreated control wells received an equivalent volume of sterile water. The plate was further incubated for 24 h under the same conditions. Cytotoxicity was then assessed using the 3-(4,5-dimethylthiazol-2-yl)-2,5-diphenyltetrazolium bromide (MTT) assay. The spent medium containing the test compounds was discarded, and 125 µL of DMEM containing 1 mg/mL MTT (Merck Life Science S.r.l.) was added to each well. The plate was incubated in the dark for 4 h at 37 °C with 5 % CO_2. Following incubation, the solution was carefully removed to avoid the loss of MTT formazan crystals, and each well was gently washed with 100 µL of sterile PBS. Then, 100 µL of IGEPAL (Sigma) (10 % *w*/*v* in 10 mM HCl) was added to each well to solubilize the formazan crystals, and the plate was incubated overnight at 37 °C with 5 % CO_2. The next day, absorbance was measured at 570 nm using a Nanoquant Infinite-M200Pro plate reader (Tecan). Cell viability was calculated by normalizing absorbance values to the untreated control wells, which were set as 100 % viability. Results represent the mean of five independent experiments, each performed in triplicate ($n = 15$).

CRediT authorship contribution statement

Francesca Albini: Writing – original draft, Data curation. **Barbara Biondi:** Writing – review & editing, Data curation, Conceptualization. **Adriana Di Stasi:** Methodology, Data curation. **Andrea Schivo:** Methodology. **Mario Mardirossian:** Writing – review & editing, Data curation. **Marco Scocchi:** Writing – review & editing, Conceptualization. **Cristina Peggion:** Writing – review & editing, Writing – original draft, Supervision, Conceptualization.

Declaration of competing interest

The authors declare the following financial interests/personal relationships which may be considered as potential competing interests: Cristina Peggion reports financial support was provided by INF- ACT, PNRR program (C93C22005170007, PE_00000007 - SP. 5). Reports a relationship with that includes:. Has patent pending to. If there are other authors, they declare that they have no known competing financial interests or personal relationships that could have appeared to influence the work reported in this paper.

Acknowledgements

This study was supported by the One Health Basic and Translational Research Actions (INF- ACT), PNRR program (C93C22005170007, PE_00000007 - SP. 5) and by the Department of Chemical Sciences, University of Padova (SID 2021 "bio HAPE").

Appendix A. Supplementary data

Supplementary data to this article can be found online at https://doi.org/10.1016/j.bioorg.2025.108715.

Data availability

Data will be made available on request.

References

[1] M. Magana, M. Pushpanathan, A.L. Santos, L. Leanse, M. Fernandez, A. Ioannidis, M.A. Giulianotti, Y. Apidianakis, S. Bradfute, A.L. Ferguson, A. Cherkasov, M. N. Seleem, C. Pinilla, C. de la Fuente-Nunez, T. Lazaridis, T. Dai, R.A. Houghten, R. E.W. Hancock, G.P. Tegos, The value of antimicrobial peptides in the age of resistance, Lancet Infect. Dis. 20 (9) (2020) e216–e230, https://doi.org/10.1016/S1473-3099(20)30327-3.

[2] C.L. Ventola, The antibiotic resistance crisis: part 1: causes and threats, P t 40(4), 2015, pp. 277–283.

[3] N.J. Afacan, A.T.Y. Yeung, O.M. Pena, R.E.W. Hancock, Therapeutic potential of host defense peptides in antibiotic-resistant infections, Curr. Pharm. Design 18 (6) (2012) 807–819, https://doi.org/10.2174/138161212799277617.

[4] X. Kang, F. Dong, C. Shi, S. Liu, J. Sun, J. Chen, H. Li, H. Xu, X. Lao, H. Zheng, DRAMP 2.0, an updated data repository of antimicrobial peptides, Scientific Data 6 (1) (2019) 148, https://doi.org/10.1038/s41597-019-0154-y.

[5] M. Mahlapuu, J. Håkansson, L. Ringstad, C. Björn, Antimicrobial peptides: an emerging category of therapeutic agents, Front. Cell. Infect. Microbiol. 6 (2016), https://doi.org/10.3389/fcimb.2016.00194.

[6] N. Mookherjee, M.A. Anderson, H.P. Haagsman, D.J. Davidson, Antimicrobial host defence peptides: functions and clinical potential, Nat. Rev. Drug Discov. 19 (5) (2020) 311–332, https://doi.org/10.1038/s41573-019-0058-8.

[7] M.R. Scheenstra, M. van den Belt, J.L.M. Tjeerdsma-van Bokhoven, V.A. F. Schneider, S.R. Ordonez, A. van Dijk, E.J.A. Veldhuizen, H.P. Haagsman, Cathelicidins PMAP-36, LL-37 and CATH-2 are similar peptides with different modes of action, Sci. Rep. 9 (1) (2019) 4780, https://doi.org/10.1038/s41598-019-41246-6.

[8] A. Tossi, L. Sandri, A. Giangaspero, Amphipathic, alpha-helical antimicrobial peptides, Biopolymers 55 (1) (2000) 4–30, https://doi.org/10.1002/1097-0282(2000)55:1<4::AID-BIP30>3.0.CO;2-M.

[9] A.T.Y. Yeung, S.L. Gellatly, R.E.W. Hancock, Multifunctional cationic host defence peptides and their clinical applications, Cell. Mol. Life Sci. 68 (13) (2011) 2161–2176, https://doi.org/10.1007/s00018-011-0710-x.

[10] M.-A. Sani, F. Separovic, How membrane-active peptides get into lipid membranes, Acc. Chem. Res. 49 (6) (2016) 1130–1138, https://doi.org/10.1021/acs.accounts.6b00074.

[11] J. Agier, M. Efenberger, E. Brzezińska-Błaszczyk, Review paperCathelicidin impact on inflammatory cells, Central European Journal of Immunology 40 (2) (2015) 225–235, https://doi.org/10.5114/ceji.2015.51359.

[12] B. Ramanathan, E.G. Davis, C.R. Ross, F. Blecha, Cathelicidins: microbicidal activity, mechanisms of action, and roles in innate immunity, Microbes Infect. 4 (3) (2002) 361–372, https://doi.org/10.1016/S1286-4579(02)01549-6.

[13] R.M. Van Harten, E. Van Woudenbergh, A. Van Dijk, H.P. Haagsman, Cathelicidins: immunomodulatory antimicrobials, Vaccines 6 (3) (2018) 63.

[14] P. Storici, M. Scocchi, A. Tossi, R. Gennaro, M. Zanetti, Chemical synthesis and biological activity of a novel antibacterial peptide deduced from a pig myeloid cDNA, FEBS Lett. 337 (3) (1994) 303–307, https://doi.org/10.1016/0014-5793(94)80214-9.

[15] J. Zhou, Y. Liu, T. Shen, L. Chen, C. Zhang, K. Cai, C. Liao, C. Wang, Antimicrobial activity of the antibacterial peptide PMAP-36 and its analogues, Microb. Pathog. 136 (2019) 103712, https://doi.org/10.1016/j.micpath.2019.103712.

[16] M.D. Balhuizen, C.M. Versluis, R.M. van Harten, E.F. de Jonge, J.F. Brouwers, C.H. A. van de Lest, E.J.A. Veldhuizen, J. Tommassen, H.P. Haagsman, PMAP-36 reduces the innate immune response induced by Bordetella bronchiseptica-derived outer membrane vesicles, Current Research in Microbial Sciences 2 (2021) 100010, https://doi.org/10.1016/j.crmicr.2020.100010.

[17] M. Mardirossian, A. Pompilio, V. Crocetta, S. De Nicola, F. Guida, M. Degasperi, R. Gennaro, G. Di Bonaventura, M. Scocchi, In vitro and in vivo evaluation of BMAP-derived peptides for the treatment of cystic fibrosis-related pulmonary infections, Amino Acids 48 (9) (2016) 2253–2260, https://doi.org/10.1007/s00726-016-2266-4.

[18] M. Benincasa, B. Skerlavaj, R. Gennaro, A. Pellegrini, M. Zanetti, In vitro and in vivo antimicrobial activity of two alpha-helical cathelicidin peptides and of their synthetic analogs, Peptides 24 (11) (2003) 1723–1731, https://doi.org/10.1016/j.peptides.2003.07.025.

[19] Q.Y. Zhang, Z.B. Yan, Y.M. Meng, X.Y. Hong, G. Shao, J.J. Ma, X.R. Cheng, J. Liu, J. Kang, C.Y. Fu, Antimicrobial peptides: mechanism of action, activity and clinical potential, Mil. Med. Res. 8 (1) (2021) 48, https://doi.org/10.1186/s40779-021-00343-2.

[20] Y. Lv, J. Wang, H. Gao, Z. Wang, N. Dong, Q. Ma, A. Shan, Antimicrobial properties and membrane-active mechanism of a potential α-helical antimicrobial derived from cathelicidin PMAP-36, PLoS One 9 (1) (2014) e86364, https://doi.org/10.1371/journal.pone.0086364.

[21] M. Scocchi, I. Zelezetsky, M. Benincasa, R. Gennaro, A. Mazzoli, A. Tossi, Structural aspects and biological properties of the cathelicidin PMAP-36, FEBS J. 272 (17) (2005) 4398–4406, https://doi.org/10.1111/j.1742-4658.2005.04852.x.

[22] J.A.E. Veldhuizen, R.M. Scheenstra, L.M.J. Tjeerdsma-van Bokhoven, M. Coorens, A.F.V. Schneider, J.F. Bikker, A. van Dijk, P.H. Haagsman, Antimicrobial and immunomodulatory activity of PMAP-23 derived peptides, Protein Pept. Lett. 24 (7) (2017) 609–616, https://doi.org/10.2174/0929866524666170428150925.

[23] Y.F. Lyu, Y. Yang, X.T. Lyu, N. Dong, A.S. Shan, Antimicrobial activity, improved cell selectivity and mode of action of short PMAP-36-derived peptides against bacteria and Candida, Sci. Rep. 6 (2016) 12, https://doi.org/10.1038/srep27258.

[24] B. Biondi, L. de Pascale, M. Mardirossian, A. Di Stasi, M. Favaro, M. Scocchi, C. Peggion, Structural and biological characterization of shortened derivatives of the cathelicidin PMAP-36, Sci. Rep. 13 (1) (2023), https://doi.org/10.1038/s41598-023-41945-1.

[25] C. Toniolo, M. Crisma, F. Formaggio, C. Peggion, Control of peptide conformation by the Thorpe-Ingold effect (C^{α}-tetrasubstitution), Biopolymers (Pept Sci) 60 (2001) 396–419, https://doi.org/10.1002/1097-0282(2001)60:6<396::AID-BIP10184>3.0.CO;2-7.

[26] I.L. Karle, P. Balaram, Structural characteristics of α-helical peptide molecules containing Aib residues, Biochemistry 29 (1990) 6747–6756, https://doi.org/10.1021/bi00481a001.

[27] G. Valle, M. Crisma, C. Toniolo, R. Beisswenger, A. Rieker, G. Jung, First observation of a helical peptide containing a chiral residue without a preferred screw sense, J. Am. Chem. Soc. 111 (17) (1989) 6828–6833, https://doi.org/10.1021/ja00199a051.

[28] S. Yang, C.W. Lee, H.J. Kim, H.H. Jung, J.I. Kim, S.Y. Shin, S.H. Shin, Structural analysis and mode of action of BMAP-27, a cathelicidin-derived antimicrobial peptide, Peptides 118 (2019) 170106, https://doi.org/10.1016/j.peptides.2019.170106.

[29] M. Mardirossian, A. Pompilio, M. Degasperi, G. Runti, S. Pacor, G. Di Bonaventura, M. Scocchi, D-BMAP18 antimicrobial peptide is active in vitro, Resists to Pulmonary Proteases but Loses Its Activity in a Murine Model of Pseudomonas aeruginosa Lung Infection, Front Chem 5 (2017) 40, https://doi.org/10.3389/fchem.2017.00040.

[30] E.F. Haney, R.E.W. Hancock, Peptide Design for Antimicrobial and Immunomodulatory Applications, Biopolymers 100 (6) (2013) 572–583, https://doi.org/10.1002/bip.22250.

[31] A. Mulukutla, R. Shreshtha, V. Kumar Deb, P. Chatterjee, U. Jain, N. Chauhan, Recent advances in antimicrobial peptide-based therapy, Bioorg. Chem. 145 (2024) 107151, https://doi.org/10.1016/j.bioorg.2024.107151.

[32] R. Tugyi, K. Uray, D. Iván, E. Fellinger, A. Perkins, F. Hudecz, Partial D-amino acid substitution: improved enzymatic stability and preserved ab recognition of a MUC2 epitope peptide, Proc. Natl. Acad. Sci. 102 (2) (2005) 413–418, https://doi.org/10.1073/pnas.0407677102.

[33] L. Yan, Y. Ke, Y. Kan, D. Lin, J. Yang, Y. He, L. Wu, New insight into enzymatic hydrolysis of peptides with site-specific amino acid d-isomerization, Bioorg. Chem. 105 (2020) 104389, https://doi.org/10.1016/j.bioorg.2020.104389.

[34] Z. Feng, B. Xu, Inspiration from the mirror: D-amino acid containing peptides in biomedical approaches, Biomol. Concepts 7 (3) (2016) 179–187, https://doi.org/10.1515/bmc-2015-0035.

[35] D. Wade, A. Boman, B. Wåhlin, C.M. Drain, D. Andreu, H.G. Boman, R. B. Merrifield, All-D amino acid-containing channel-forming antibiotic peptides, Proc. Natl. Acad. Sci. 87 (12) (1990) 4761–4765, https://doi.org/10.1073/pnas.87.12.4761.

[36] S. Kapil, V. Sharma, D-amino acids in antimicrobial peptides: a potential approach to treat and combat antimicrobial resistance, Can. J. Microbiol. 67 (2) (2021) 119–137, https://doi.org/10.1139/cjm-2020-0142 %M 32783775.

[37] B. Biondi, B. Casciaro, A. Di Grazia, F. Cappiello, V. Luca, M. Crisma, M. L. Mangoni, Effects of Aib residues insertion on the structural–functional properties of the frog skin-derived peptide esculentin-1a(1−21)NH2, Amino Acids 49 (1) (2017) 139–150, https://doi.org/10.1007/s00726-016-2341-x.

[38] Y. Marciano, N. Nayeem, D. Dave, R.V. Ulijn, M. Contel, N-acetylation of biodegradable supramolecular peptide Nanofilaments selectively enhances their proteolytic stability for targeted delivery of gold-based anticancer agents, ACS Biomater Sci. Eng. 9 (6) (2023) 3379–3389, https://doi.org/10.1021/acsbiomaterials.3c00312.

[39] R. Behrendt, P. White, J. Offer, Advances in Fmoc solid-phase peptide synthesis, J. Pept. Sci. 22 (1) (2016) 4–27, https://doi.org/10.1002/psc.2836.

[40] C.E. MacPhee, M.A. Perugini, W.H. Sawyer, G.J. Howlett, Trifluoroethanol induces the self-association of specific amphipathic peptides, FEBS Lett. 416 (3) (1997) 265–268, https://doi.org/10.1016/S0014-5793(97)01224-6.

[41] M.K. Luidens, J. Figge, K. Breese, S. Vajda, Predicted and trifluoroethanol-induced alpha-helicity of polypeptides, Biopolymers 39 (3) (1996) 367–376, https://doi.org/10.1002/(sici)1097-0282(199609)39:3%3c367::Aid-bip8%3e3.0.Co;2-m.

[42] J.K. Myers, C.N. Pace, J.M. Scholtz, Trifluoroethanol effects on helix propensity and electrostatic interactions in the helical peptide from ribonuclease T1, Protein Sci. 7 (2) (1998) 383–388, https://doi.org/10.1002/pro.5560070219.

[43] L. Whitmore, B.A. Wallace, Protein secondary structure analyses from circular dichroism spectroscopy: methods and reference databases, Biopolymers 89 (5) (2008) 392–400, https://doi.org/10.1002/bip.20853.

[44] H. Sato, J.B. Feix, Peptide–membrane interactions and mechanisms of membrane destruction by amphipathic α-helical antimicrobial peptides, Biochimica et Biophysica Acta (BBA), Biomembranes 1758 (9) (2006) 1245–1256, https://doi.org/10.1016/j.bbamem.2006.02.021.

[45] C. Toniolo, M. Crisma, F. Formaggio, C. Peggion, R.F. Epand, R.M. Epand, Lipopeptaibols, a novel family of membrane active, antimicrobial peptides, Cell. Mol. Life Sci. 58 (9) (2001) 1179–1188, https://doi.org/10.1007/PL00000932.

[46] N.H. Andersen, Z. Liu, K.S. Prickett, Efforts toward deriving the CD spectrum of a 310 helix in aqueous medium, FEBS Lett. 399 (1–2) (1996) 47–52, https://doi.org/10.1016/S0014-5793(96)01279-3.

[47] C. Toniolo, A. Polese, F. Formaggio, M. Crisma, J. Kamphuis, Circular dichroism Spectrum of a peptide 310-Helix, J. Am. Chem. Soc. 118 (11) (1996) 2744–2745, https://doi.org/10.1021/ja9537383.

[48] M.C. Manning, R.W. Woody, Theoretical CD studies of polypeptide helices: examination of important electronic and geometric factors, Biopolymers 31 (5) (1991) 569–586, https://doi.org/10.1002/bip.360310511.

[49] D. Núñez-Villanueva, Revisiting 310-helices: biological relevance, mimetics and applications, Exploration of Drug Science 2 (1) (2024) 6–37, https://doi.org/10.37349/eds.2024.00034.

[50] R.W. Woody, Theory of circular dichroism of proteins, in: G.D. Fasman (Ed.), Circular Dichroism and the Conformational Analysis of Biomolecules, Springer US, Boston, MA, 1996, pp. 25–67, https://doi.org/10.1007/978-1-4757-2508-7_2.

[51] I. Jahan, S.D. Kumar, S.Y. Shin, C.W. Lee, S.-H. Shin, S. Yang, Multifunctional properties of BMAP-18 and its aliphatic analog against drug-resistant Bacteria, Pharmaceuticals 16 (10) (2023) 1356, https://doi.org/10.3390/ph16101356.

[52] C. Toniolo, E. Benedetti, The polypeptide 310-helix, Trends Biochem. Sci. 16 (9) (1991) 350–353, https://doi.org/10.1016/0968-0004(91)90142-i.

[53] K. Wüthrich, NMR of Proteins and Nucleic Acids, 1991.

[54] G.L. Millhauser, Views of helical peptides: a proposal for the position of 310-Helix along the thermodynamic folding pathway, Biochemistry 34 (12) (1995) 3873–3877, https://doi.org/10.1021/bi00012a001.

[55] G.L. Millhauser, C.J. Stenland, P. Hanson, K.A. Bolin, F.J.M. van de Ven, Estimating the relative populations of 310-helix and α-helix in ala-rich peptides: a hydrogen exchange and high field NMR study11Edited by P. E. Wright, J. Mol. Biol. 267 (4) (1997) 963–974, https://doi.org/10.1006/jmbi.1997.0923.

[56] J.V. Olsen, S.-E. Ong, M. Mann, Trypsin cleaves exclusively C-terminal to arginine and lysine residues*, Mol. Cell. Proteomics 3 (6) (2004) 608–614, https://doi.org/10.1074/mcp.T400003-MCP200.

[57] W. Ma, C. Tang, L. Lai, Specificity of trypsin and chymotrypsin: loop-motion-controlled dynamic correlation as a determinant, Biophys. J. 89 (2) (2005) 1183–1193, https://doi.org/10.1529/biophysj.104.057158.

[58] F. Fathi, B. Alizadeh, M.V. Tabarzad, M. Tabarzad, Important structural features of antimicrobial peptides towards specific activity: trends in the development of efficient therapeutics, Bioorg. Chem. 149 (2024) 107524, https://doi.org/10.1016/j.bioorg.2024.107524.

[59] B. Skerlavaj, R. Gennaro, L. Bagella, L. Merluzzi, A. Risso, M. Zanetti, Biological characterization of two novel cathelicidin-derived peptides and identification of structural requirements for their antimicrobial and cell lytic activities, J. Biol. Chem. 271 (45) (1996) 28375–28381, https://doi.org/10.1074/jbc.271.45.28375.

[60] R.F. Epand, R.M. Epand, V. Monaco, S. Stoia, F. Formaggio, M. Crisma, C. Toniolo, The antimicrobial peptide trichogin and its interaction with phospholipid membranes, Eur. J. Biochem. 266 (3) (1999) 1021–1028, https://doi.org/10.1046/j.1432-1327.1999.00945.x.

[61] E.K. Lee, Y.C. Kim, Y.H. Nan, S.Y. Shin, Cell selectivity, mechanism of action and LPS-neutralizing activity of bovine myeloid antimicrobial peptide-18 (BMAP-18) and its analogs, Peptides 32 (6) (2011) 1123–1130, https://doi.org/10.1016/j.peptides.2011.03.024.

[62] M. De Zotti, B. Biondi, C. Peggion, F. Formaggio, Y. Park, K.-S. Hahm, C. Toniolo, Trichogin GA IV: a versatile template for the synthesis of novel Peptaibiotics, Org. Biomol. Chem. 10 (6) (2012) 1285–1299, https://doi.org/10.1039/C1OB06178J.

[63] C. Toniolo, C. Peggion, M. Crisma, F. Formaggio, X.Q. Shui, D.S. Eggleston, Structure determination of racemic Trichogin GA IV using centrosymmetric crystals, Nat. Struct. Biol. 1 (12) (1994) 908–914, https://doi.org/10.1038/nsb1294-908.

[64] C. Peggion, F. Formaggio, M. Crisma, R.F. Epand, R.M. Epand, C. Toniolo, Trichogin: a paradigm for Lipopeptaibols, J. Pept. Sci. 9 (11−12) (2003) 679–689, https://doi.org/10.1002/psc.500.

[65] H. Bui Thi Phuong, H. Doan Ngan, B. Le Huy, H. Vu Dinh, H. Luong Xuan, The amphipathic design in helical antimicrobial peptides, ChemMedChem 19 (7) (2024) e202300480, https://doi.org/10.1002/cmdc.202300480.

[66] E.S. Salnikov, J. Raya, M. De Zotti, E. Zaitseva, C. Peggion, G. Ballano, C. Toniolo, J. Raap, B. Bechinger, Alamethicin supramolecular Organization in Lipid Membranes from ^{19}F solid-state NMR, Biophys. J. 111 (11) (2016) 2450–2459, https://doi.org/10.1016/j.bpj.2016.09.048.

[67] A. Pompilio, V. Crocetta, M. Scocchi, S. Pomponio, V. Di Vincenzo, M. Mardirossian, G. Gherardi, E. Fiscarelli, G. Dicuonzo, R. Gennaro, G. Di Bonaventura, Potential novel therapeutic strategies in cystic fibrosis: antimicrobial and anti-biofilm activity of natural and designed α-helical peptides against Staphylococcus aureus, Pseudomonas aeruginosa, and Stenotrophomonas maltophilia, BMC Microbiol. 12 (1) (2012) 145, https://doi.org/10.1186/1471-2180-12-145.

[68] N.M. O'Brien-Simpson, N. Pantarat, T.J. Attard, K.A. Walsh, E.C. Reynolds, A rapid and quantitative flow cytometry method for the analysis of membrane disruptive antimicrobial activity, PLoS One 11 (3) (2016) e0151694, https://doi.org/10.1371/journal.pone.0151694.

[69] T.L. Hwang, A.J. Shaka, Water suppression that works, Excitation Sculpting Using Arbitrary Wave-Forms and Pulsed-Field Gradients, Journal of Magnetic Resonance, Series A 112 (2) (1995) 275–279, https://doi.org/10.1006/jmra.1995.1047.

[70] M. Rance, O.W. Sørensen, G. Bodenhausen, G. Wagner, R.R. Ernst, K. Wüthrich, Improved spectral resolution in COSY 1H NMR spectra of proteins via double quantum filtering, Biochem. Biophys. Res. Commun. 117 (2) (1983) 479–485, https://doi.org/10.1016/0006-291X(83)91225-1.

[71] C. Griesinger, G. Otting, K. Wuethrich, R.R. Ernst, Clean TOCSY for proton spin system identification in macromolecules, J. Am. Chem. Soc. 110 (23) (1988) 7870–7872, https://doi.org/10.1021/ja00231a044.
[72] H. Jenssen, S.I. Aspmo, Serum stability of peptides, in: L. Otvos (Ed.), Peptide-Based Drug Design, Humana Press, Totowa, NJ, 2008, pp. 177–186, https://doi.org/10.1007/978-1-59745-419-3_10.
[73] T.O. Koller, M.J. Berger, M. Morici, H. Paternoga, T. Bulatov, A. Di Stasi, T. Dang, A. Mainz, K. Raulf, C. Crowe-McAuliffe, M. Scocchi, M. Mardirossian, B. Beckert, N. Vázquez-Laslop, A.S. Mankin, R.D. Süssmuth, D.N. Wilson, Paenilamicins are context-specific translocation inhibitors of protein synthesis, Nat. Chem. Biol. 20 (12) (2024) 1691–1700, https://doi.org/10.1038/s41589-024-01752-9.